Agricultural and Forest Meteorology 328 (2023) 109257

Contents lists available at ScienceDirect

Agricultural and Forest Meteorology

journal homepage: www.elsevier.com/locate/agrformet

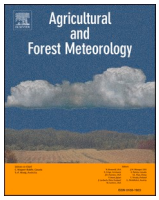

# Rainfall interception measurements and modeling in a semiarid evergreen spruce (*Picea crassifolia*) forest

Junjun Yang [a,b,*], Zhibin He [b], Jianmin Feng [a], Pengfei Lin [b], Jun Du [b], Lingxia Guo [a], Yufeng Liu [a], Jialiang Yan [c]

[a] College of Geography and Environment, Xianyang Normal University, Xianyang 712000, China
[b] Linze Inland River Basin Research Station, Chinese Ecosystem Research Network, Key Laboratory of Eco-hydrology of Inland River Basin, Northwest Institute of Eco-Environment and Resources, Chinese Academy of Sciences, Lanzhou 730000, China
[c] Institute of Geography Science, Taiyuan Normal University, Jinzhong 030619, Shanxi, China

ARTICLE INFO

*Keywords:*
Interception loss
Rainfall partitioning
Modeling
Throughfall
Stemfall
Qinghai spruce forest

ABSTRACT

Rainfall interception is a critical source of water in arid and semiarid mountain forests. Interception loss (*I*) in mountain forests determines the ecohydrological function of a watershed, and this is particularly important in arid and semi-arid regions that rely on runoff yield to balance human and ecosystem water needs. Here, we measured gross rainfall (*P*), throughfall (*Tf*), and stemflow (*Sf*) from May 2020 to September 2021, and leaf area index (LAI), canopy structural parameters, and meteorological data within a *Picea crassifolia* (*P. crassifolia*) forest in the Qilian Mountains of northwestern China. Throughfall and canopy interception accounted for 56.4 and 35.2% of the 745.5 mm cumulative rainfall input during the two growing seasons, respectively. Stemflow of up to 13.6% of total rainfall events occurred when the amount of $P > 30$ mm, and canopy storage capacity (*S*) was 2.0 mm. Based on the parameters derived from a regression equation between *Tf* vs. *P* and a trial-and-error calibration scheme, three of the physical models, the Návar, reformulated Gash, and Liu, performed very well both for event-based (NSE $> 0.8$) and total-based (NSE $> 0.92$) *I*; a larger deviation was found during large rainfall events, especially for the reformulated Gash model. These results indicated that the power Návar and the reformulated Liu model are best for event-based and total-based *I* modeling, respectively, in spruce forests in this semi-arid region.

## 1. Introduction

The interception fraction of rainfall (*I*) modifies surface-atmosphere energy and hydrological budgets (Raz-Yaseef et al., 2010; Rotenberg and Yakir, 2010), therefore, it is critical in arid and semi-arid regions where water is a limiting factor for ecosystem stability and economic development (Ma et al., 2020; Nazari et al., 2020; Qubaja et al., 2020). Rainfall intercepted in dry environments depends on water partitioning through the forest canopy and plant water use characteristics (Fathizadeh et al., 2017; Jian et al., 2019; Sadeghi et al., 2015). Rainfall intercepted by the canopy may be lost via evaporation, but the volume of loss varies greatly with tree species, forest density, canopy structure (Linhoss and Siegert, 2016), and climatic conditions (Liu, 1997). It is increasingly recognized that a better understanding of water use patterns and their response to climate change depends on our ability to partition rainfall and simulate the dynamics of its fractions.

The main factors influencing *I* are canopy storage capacity (*S*) (Liu, 1997), canopy saturation point, canopy cover fraction (*c*) (Gash, 1979; Rutter et al., 1972), free throughfall coefficient (*p*), average wet canopy evaporation rate, and rainfall distribution (Eliades et al., 2022). The amount of *S*, canopy saturation point, and canopy cover fraction depends on vegetation type for evergreen forests, and the growing season for deciduous forests, while the average wet canopy evaporation and interception losses are highly weather-related. Therefore, derivation of hydrological parameters from observation records is one of the most important links in regional hydrological process research (Deguchi et al., 2006; Motahari et al., 2013).

The majority of interception models focus on the cumulative amounts and perform poorly with individual values of rainfall interception (Muzylo et al., 2009); this could be due to temporal variability in input data and the mathematical theory behind these techniques (Návar, 2019). An independent analytical model, developed by Návar

* Corresponding author.
*E-mail address:* junjun_yang@126.com (J. Yang).

https://doi.org/10.1016/j.agrformet.2022.109257
Received 7 June 2022; Received in revised form 26 October 2022; Accepted 21 November 2022
Available online 25 November 2022

**Table 1**
Range, frequency, and the average value of gross rainfall (*P*) during the observation period at 3000 m elevation. ± value denotes standard error (Std.), *I/P* means the relative interception loss between *I* (mm) and *P* (mm).

| Observation period | Rainfall class (mm) | Frequency (N) | Frequency percentage (%) | Precipitation percentage (%) | Average (mm) | I/P (%) | Description |
|---|---|---|---|---|---|---|---|
| Growing season in 2020 and 2021 | 0–4.9 | 22 | 37.3 | 7.9 | 2.69±1.31 | 62.2 ± 18.0 | Very small (C1) |
| | 5–9.9 | 12 | 20.3 | 10.8 | 6.71±1.33 | 54.3 ± 5.7 | Small (C2) |
| | 10–14.9 | 4 | 6.8 | 6.7 | 12.41±1.86 | 46.0 ± 7.1 | Middle (C3) |
| | 15–19.9 | 8 | 13.6 | 17.9 | 16.67±1.15 | 48.2 ± 6.6 | Large (C4) |
| | 20–29.9 | 6 | 10.2 | 20.2 | 25.15±3.42 | 40.3 ± 11.4 | Very large (C5) |
| | 30–51.25 | 7 | 11.9 | 36.5 | 38.83±7.81 | 35.5 ± 4.2 | Storm (C6) |

(2020), exhibits a very good performance with individual events and cumulative values of *I*. Linear and power equations can be analyzed when predicting *I* as a function of gross rainfall for a particular climate and forest type. Currently, there are almost 17 published *I* models, of which the sparse Gash (Gash, 1979; Gash et al., 1995; Sadeghi et al., 2015) and the re-formulated Liu (Liu, 1997; Muzylo et al., 2009) models are the most frequently used in simulation of the world's forests (Linhoss and Siegert, 2016). The Návar model expands the traditional drip equations to predict *I, S* and rainfall features, but it has yet to be fully evaluated for dryland forests (Návar, 2019, 2020).

Additionally, there is an urgent need for a comparison of the Návar, Gash, and Liu models for robustness and applicability to rainfall partitioning, especially for dryland forest plantations. Parameters for model development are commonly derived from reference values for individual tree types or from coefficients of regression equations for *I* vs. *P* or *Tf* vs. *P* (Carlyle-Moses and Price, 2007; Motahari et al., 2013), both of which often result in large deviations. As a consequence, new calibration methods are needed for model parameterization. An improved understanding of model applicability and of effects of parameter acquisition on interception loss will enhance accuracy of water-oriented prediction and management of semiarid forest plantations.

In this study, we measured *P, Tf*, and *Sf* in a fixed 240 $m^2$ plot at 3000 m elevation from May 2020 to October 2021. We also determined leaf area index (LAI), meteorological data at 30-minute intervals, and soil water content in a *P. crassifolia* forest in the Qilian Mountains of northwestern China. Our objective in this study was to: (1) determine canopy structure variables and partition interception parameters in a *P. crassifolia* forest, (2) derive an optimal model parameterization scheme, and (3) validate the three primary physical interception models based on the adapted stand parameters.

## 2. Materials and methods

### 2.1. Study area and measurements

The study was conducted in Pailugou catchment, located 50 km south of Zhangye City, Gansu Province (100°17′ E, 38°24′ N), China. The area is part of the northern Qilian Mountains and has continental arid climate with hot and rainy seasons. Mean annual precipitation was 384 mm from 2000 to 2020 at 2700 m, of which nearly 65% fell during the summer. Mean annual air temperature is 0.5 °C; pan evaporation is 1051.7 mm. *P. crassifolia* is the only tree species in the study area; it is primarily distributed at elevations between 2650 and 3400 m, and ranges in age from 80 to 120 years old. Moss (*Abietinella abietina*) accounts for 95% cover of the forest floor, with a thickness of 10 to 30 cm. The soil is gray-drab with a field water capacity of 53.8%, bulk density of 850 kg $m^{-3}$, and depth of 70 cm (Chang et al., 2014).

### 2.2. Gross precipitation (P), throughfall (Tf), stemflow (Sf) and interception (I)

*P* was measured using one manual rain-gage (20 cm diameter) located in a nearby forest gap (< 20 m away from the plot). A rain event was defined as a period when *P* was > 0.5 mm; rain events were separated by a drying time of more than 10 h (Sadeghi et al., 2015). Fifty-nine rainfall events were observed during the growing season of 2020 and 2021. Based on the amounts measured for past rainfalls in the Qilian Mountains, *P* was divided into six classes (Table 1). Surface runoff was measured in a 5 × 10 m runoff field within the plot. To quantify and evaluate rainfall intensity and duration, two HOBO RG3-M automatic precipitation sensors (470 MacArthur Blvd., Bourne, MA 02532, U.S.) were installed at the observation site to continuously collect and record rainfall at 30-min intervals; sensitivity of the sensor was 0.2 mm.

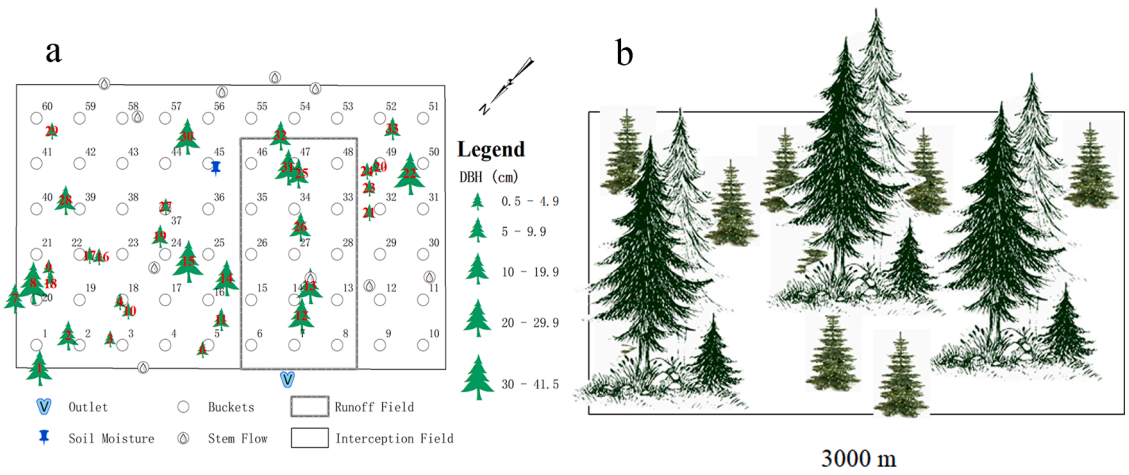


**Fig. 1.** Map of the sampling instruments within the plot at 3000 m elevation. (a) layout of collectors and sampling trees during the growing seasons in 2020 and 2021; (b) distribution of diameter at breast height (DBH) within the plot.

**Table 2**
DBH and LAI distribution statistics at the stemflow-collector position in the study plot at 3000 m elevation.

| Variables | DBH (cm) | LAI |
|---|---|---|
| N | 32 | 60 |
| Mean | 12.9 ± 12.6 | 2.72 |
| Variance | 159.1 | 0.28 |
| Range | 41.0 | 2.58 |
| Minimum | 0.5 | 1.58 |
| Maximum | 41.5 | 4.16 |

Note: N is the number of samples.

*Tf* and *Sf* were measured in a 12 × 20 m plot at an elevation of 3000 m (Fig. 1). Sixty cylindrical throughfall collectors made of stainless steel (height = 24 cm, diameter = 20 cm) were evenly distributed across the plot area at an interval of 2 m, for the purpose of long-term observation and analysis of individual interception events (Calder, 1976; Crockford and Richardson, 2000). *Tf* was collected within 2 *h* after each rainfall in graduated cylinders (accurate to 0.1 cm) suspended on 10 evenly-distributed trees at breast height (1.5 m above ground).

*Sf* data were obtained from direct measurements, and the collectors for *Sf* were built following the recommendations of Pypker et al. (2012). According to He et al. (2014), *Sf* is present in this area primarily with heavy rainfall events, thus the collector volume for *Sf* measurements was 20 L.

Soil moisture was monitored at 30 min intervals with EM50 (Decagon, Inc. Decagon, USA), calibrated against the gravimetric method at five soil depths (5, 10, 20, 40, and 60 cm). *P, Tf*, and *Sf* measurements were recorded only during the frost-free season (typically May to September).

Interception losses (*I*) are generally determined as the difference between *P* and the sum of *Tf* and *Sf* (Eq. (1)) (Junqueira Junior et al., 2019; Prasad Ghimire et al., 2017). Linear regression equations were fitted for the *Tf* vs. *P* relationship for the plot. Parameter used in the models were derived from the relationship, including the maximum forest storage capacity (*Ps*) which corresponds to *P* when *Tf* is zero and the relationship between *Tf* and *P* is linear (Gash, 1979).

$$I = P - (Tf + Sf) \tag{1}$$

### 2.3. Tree structural traits

To investigate the relationship between canopy ecohydrological parameters and tree structural traits, diameter at breast height (DBH) was measured for 32 trees, leaf area index (LAI) was determined for 60 trees, and the canopy cover fraction (*c*) at 1.3 m above each throughfall collector was determined. LAI and *c* were obtained using an LAI-2200 plant canopy analyzer (LI-COR, Inc. U.S. & Canada) in July 2021. Tree size classes were categorized as: DBH ≦ 4.9 cm, 5 – 9.9 cm, 10 – 19.9 cm, 20 – 29.9 cm, 30 – 39.9 cm, > 40 cm (Table 2).

### 2.4. Parameterization of interception components

*S*, the canopy saturation point or the water storage capacity, is the amount of *P* required to saturate the canopy (Sadeghi et al., 2015); the maximum canopy storage capacity (*Ps*) is defined as the minimum amount of rainfall the canopy can hold while saturated (Klaassen et al., 1998). *S* was derived from separate regression lines relating *P* to *Tf* for rainfalls that were either pre-sufficient (R1, $P < Ps$) or post-sufficient (R2, $P \geq Ps$) for the canopy; the value of *P* at the intersection of R1 and R2 provides an estimate of *Ps* and, the difference between *P* and *Tf* at the intersection of R1 and R2 was *S*. The slope of the regression line R1 represents the free throughfall coefficient *p*, which is defined as the proportion of rain which falls to the ground through gaps without striking the canopy (Grunicke et al., 2020). The mean wet canopy evaporation during rainfall *Ev* (mm $h^{-1}$) was estimated from a regression between *I* and *P* (Gash, 1979) (Table 3).

### 2.5. Rainfall interception modeling

#### 2.5.1. Návar model

The Návar model was developed for forest interception (*I*) and its components *S* and *Ev* during rainfall (Návar, 2020). *I* was parsed into *S* and *Er* using analytical techniques, and the model provides independent and unbiased *I* and *S* assessments; the model allows for comparisons of linear and power functions specific to the forest, climate, or rainfall conditions (Návar, 2019).

$$\mathrm{I}_{LM} = \left(\left[b_0 - kP_{in}^{c} + b_{in}P_{in}\right]\right)P_{in} + \int_{P_{in}}^{P} b_{in}\exp^{(-0.0001P)} * \partial P \tag{2}$$

$$\mathrm{I}_{PM} = \left(\left[b_0 - kP_{in}^{c} + b_{in}P_{in}\right]\right)P_{in} + \int_{P_{in}}^{P} kP^{(\pm g_1)} * \partial P \tag{3}$$

Where, $b_0$, $b_{in}$ are intercept and slope of the linear equation, k, c are the parameters of the power equation, the depth of *P* from $P = 0$ to $P = P_{in}$ is assumed to account for most of the precipitation needed to saturate the canopy, the $g_1$ value indicates the influx of advected energy and is quasi constant during most storms in dry and seasonal dry forests (Návar, 2020), and $I_{LM}$ and $I_{PM}$ are the interception loss models in the linear and power modes, respectively.

#### 2.5.2. The reformulated Gash model

The reformulated Gash canopy model estimates *I* for *n* rainfall events with sufficient volume to saturate the canopy ($P > P_s$) on an event basis (Cuartas et al., 2007; Prasad Ghimire et al., 2017); the forest parameter is kept constant, and the rainfall inputs are taken as discrete rainfall events divided by the length of intervals sufficient to dry the canopy and stems. The model estimates evaporation based on canopy area rather than on the ground area.

$$I_{\mathrm{n}} = I_{\mathrm{w}} + I_a + \left(c\frac{\overline{E}_v}{\overline{R}}\sum_{j=1}^{n}(P - P_{\mathrm{s}})\right) + \left(n' S_s + P_t\sum_{j=1}^{n-n'}(P)\right) \tag{4}$$

$$I_w = ncP_g - ncS_c \tag{5}$$

$$I_a = ncS_c \tag{6}$$

Where, $I_w$ is evaporation from the canopy when $P > P_s$; $I_a$ refers to evaporation from the canopy when throughfall stopped; $\overline{E}_v$ is the average canopy evaporation, and $\overline{R}$ is the average rainfall intensity necessary for canopy saturation when $P \geq P_s$. $P_g$ is the saturation canopy point (*Ps*), *n'* refers to the number of rainfall events with $P > S_s/P_b$, $S_s$ is

**Table 3**
Parameter value used for the three models in the present study.

| Model parameter | Návar model | Model parameter | Reformulated Gash model | Model parameter | Reformulated Liu model |
|---|---|---|---|---|---|
| $P_{in}$ (mm) | 2.37 | *Ps* (mm) | 1.84–2.0 | *Ps* (mm) | 1.16–1.46 |
| $b_0$ | 0.56 | *ER* (mm $h^{-1}$) | 0.34–0.64 | *ER* (mm $h^{-1}$) | 0.85–1.26 |
| *c* | 0.85 | *c* | 0.74–0.84 | *C* | 0.75–0.88 |
| $b_{in}$ | 0.31 | *S* (mm) | 1.41–2.68 | *Ev* (mm $h^{-1}$) | 0.08–0.25 |
| *k* | 0.30 | | | *S* (mm) | 1.20–2.12 |
| $g_1$ | 0.29 | | | *Ss* (mm) | 1.56 |

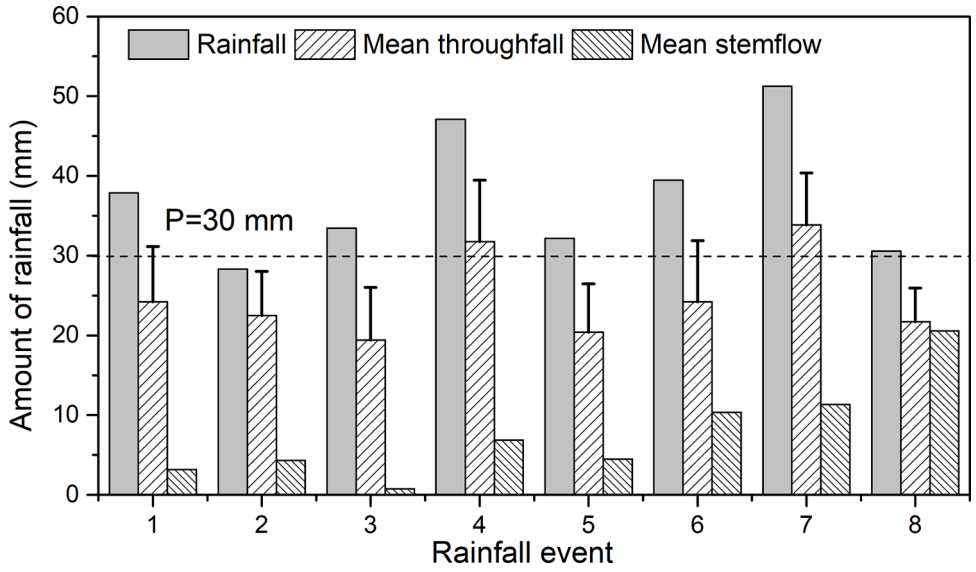


**Fig. 2.** Rainfall (*P*), mean throughfall (*Tf*) and mean stemflow (*Sf*) in the stemflow events during the two observational seasons, the dash line is a reference line with rainfall = 30 mm.

the stem storage capacity and $P_t$ is the proportion of *P* converted to *Sf*.

### 2.5.3. The reformulated Liu model

The Liu model (Liu (1997), revised by Carlyle-Moses and Price (2007), accounts for the presence of forest gaps. Drainage from the canopy starts before its saturation, and canopy saturation is exponential in nature. The model is given by Eq. (7):

$$I = \sum_{j=1}^{n}\left(c\left\{S_{cs}\left[1-\exp\left[\left(-\frac{1}{S_{cs}}\right)P\right]\right]\cdot\left[1-\frac{\overline{E}v}{\overline{R}}\right]+\frac{\overline{E}v}{\overline{R}}P\right\}\right) \quad (7)$$

$$I = c\sum_{j=1}^{m}P_j \quad (8)$$

where *n* is the total number of rainfall events, and *m* is the number of events, which are pre-sufficient to $P_s$. $S_{cs}$ (mm) is the sum of canopy and stem storage capacity (*S* and $S_s$, respectively).

## 2.6. Evaluation of model performance

Model performance was assessed using the coefficient of determination ($R^2$) to indicate the fit of the regression model between observed and simulation results. We also compared the mean relative absolute error (MRAE), and Nash-Sutcliffe efficiency (NSE) to determine the relative magnitude of the residual variance of two records (Nash and Sutcliffe, 1970).

$$R^2 = 1-\frac{\sum_{i=1}^{n}(I_i-\widehat{I}_i)^2}{\sum_{i=1}^{n}(I_i-\overline{I})^2} \quad (4)$$

$$MRAE = \frac{1}{n}\sum_{i=1}^{n}\left|\frac{(I_i-\widehat{I}_i)}{\widehat{I}_i}\right| \quad (5)$$

$$NSE = 1-\frac{\sum_{i=1}^{n}(I_i-\widehat{I}_i)^2}{\sum_{i=1}^{n}(I_i-\overline{I})^2} \quad (6)$$

where: $I_i$ is derived from measured *P, Tf*, and *Sf;* $\hat{I}$ is interception using the proposed model; *n* is the total number of measured storms during the observation period.

The performance of the model was evaluated using MRAE as follows: MRAE can range from 0 to infinity, with low numbers indicating a better performance; this is not affected by the direction of errors since absolute values are used. MRAE is a more stringent test of model performance than mean error (%) Muzylo et al. (2009). NSE determines model fit as follows: unsatisfactory (NSE ≤ 0.50), satisfactory (0.50 < NSE ≤ 0.70), good (0.70 < NSE ≤ 0.80), and very good (NSE > 0.80) (Fan et al., 2014; N. Moriasi et al., 2015). Assessin g stand water use in four coastal wetland forests using sapflow techniques

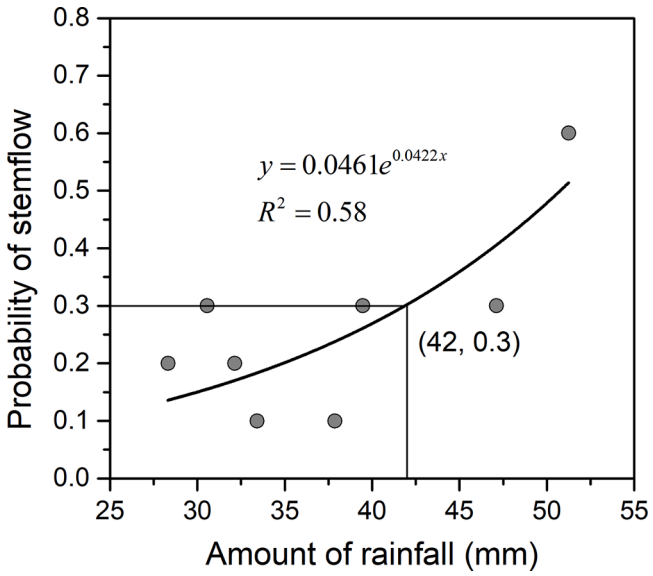


**Fig. 3.** Probability of occurrence of stemflow during the two seasons of study.

## 3. Results

### 3.1. Rainfall partitioning and model parameters

We registered 59 rainfall events between May 2020 and September 2021, with a total amount of rain of 745.5 mm and an average (±stand deviation) of 12.6 ± 12.4 mm per event (Table 1). Twenty-two events (37.3%) did not exceed 5 mm, and 20.3% events delivered between 5 and 10 mm of rain. Nearly 12% of rain events were > 30 mm, and contributed ≥ 39% of the total rainfall. The duration of a rainfall event was between 0.5 and 11.5 *h*, with an average of 2.5 *h* during the two

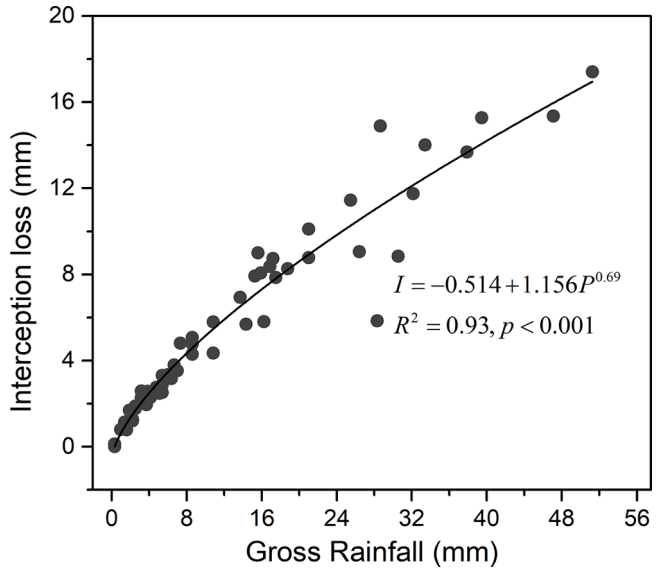


**Fig. 4.** The regression equation between gross rainfall (*P*) and interception loss (*I*).

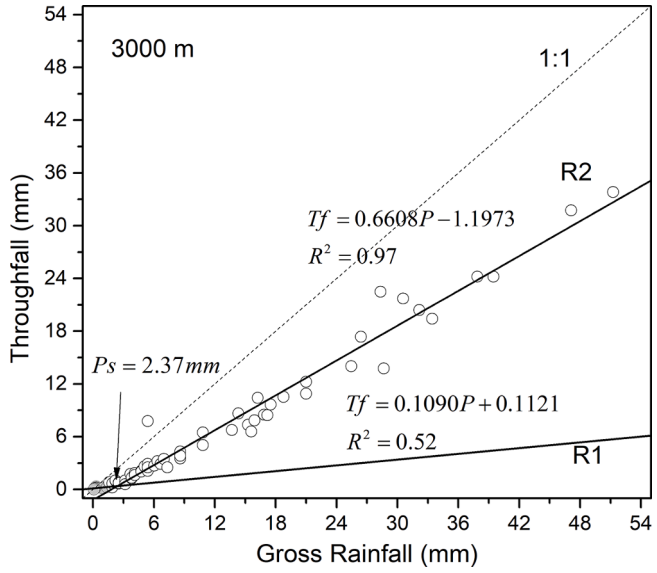


**Fig. 5.** The regression relationship between gross rainfall (*P*) and throughfall (*Tf*) for rainfall events; R1 is a fitting line when *P* is lower than canopy saturation point (*Ps*), and R2 is a fitting line when $P \geq Ps$ at 3000 m elevation.

years of study; rain intensity ranged from 0.4 to 5.8 mm $h^{-1}$, with an average of 0.7 mm $h^{-1}$ indicating that small rainfall dominates rainfall type in this region.

*Tf* and *Sf* was 420.4 and 62.8 mm, respectively, accounting for approximately 56.4 and 8.4% of the total rainfall, respectively. An *I* event totaled 262.3 mm, accounting for 35.2% of *P*. Notably, 9 of 59 (approximately 15.3%) rainfall events produced stemflow, with the amount of rainfall ranging from 28.3 to 51.2 mm (Fig. 2). Probability of stemflow was low and increased with the amount of rainfall (Fig. 3); when the amount of rainfall was 42 mm, stemflow occurred nearly 30% of time, and the relationship was an exponential function.

Event-based relative interception loss (*I*/*P*) varied between 35.5 (for C6 event) and 62.2% (for C1 event) in a power regression equation for *I* vs. *P* (Fig. 4), decreasing with increasing rainfall (Table 1) and stabilizing around *S* of the forest; there was no recharge occurrence in the study area during the two hydrological years.

**Table 4**
Summary statistics for interception (*I*) evaluation using three models for event-based and total-based rainfall during two years.

| Model | Event-based results | | | Total-based results | | |
|---|---|---|---|---|---|---|
| | $R^2$ | MRAE | NSE | $R^2$ | MRAE | NSE |
| Power Návar model | 0.93 | 0.39 | 0.90 | 0.99 | 0.09 | 0.93 |
| Reformulated Gash model | 0.93 | 0.30 | 0.80 | 0.99 | 1.03 | 0.98 |
| Reformulated Liu model | 0.93 | 0.19 | 0.92 | 0.99 | 0.00 | 0.99 |

Parameters in the Návar model were derived from values recommended for an arid and semi-arid forest in southeastern Brazil of Junqueira Junior et al. (2019); parameters used in other two models were calculated from measured values (Fig. 5). Partial parameters were determined following trial-and-error techniques (Gill et al., 2006; Návar, 2020; Nourani et al., 2014; Yang et al., 2016). We used mean *Ps* of 2.37 mm, *S* of 2.0 mm, and free throughfall coefficient *p* of 0.11 (Fig 5).

### 3.2. Model performance

The relationship between observed *I* and *I* modeled with the power Návar model exhibited an $R^2 = 0.93$, MER = 0.39, and NSE = 0.90 (Table 4 and Fig. 6), while that between observed *I* and *I* modeled with the linear model exhibited an unfavorable performance with $R^2 = 0.92$, MEAR = 0.51, and NSE = −4.04 (not shown here), indicating that the power equation model is appropriate for this area. Modeling of interception based on event (Fig. 6a) or the cumulative amount (Fig. 6b) gave similar results across the three models. The Liu model exhibited an outstanding performance with NSE = 0.92, while the reformulated Gash model had NSE = 0.80. The reformulated Gash model overestimated, while the Návar model somewhat underestimated in the high value range. The Liu model overestimated slightly in the low range. Further, the Návar and Gash models resulted in MRAE of 0.39 and 0.30, respectively, while the Liu model yielded a larger MRAE of 0.59. The cumulative *I* for the three models exhibited a consistently good fit with NSE > 0.9 (Table 4 and Fig. 6), although the Návar model was the weakest. The cumulative MRAE of the Gash model exhibited greater deviation at > 1.00. Again, the Liu model performed consistently well (MRAE=0.00) for the unbiased *I* assessments. Both Návar and reformulated Gash model overestimated event interception by an average of 0.7 mm, and the Liu model performed best with a slightly underestimated interception by event-based −0.27 mm (Table 5).

## 4. Discussion

*Stand structure and rainfall partitioning measurements.* *Tf* measurements are affected by rainfall amount, tree density, and canopy structure (Ma et al., 2020). Overall, accuracy of measurement requires an adequate number of throughfall collectors, appropriate collector position within the stand, and sufficient length of observation or number of rainfall events (Junqueira Junior et al., 2019; Prasad Ghimire et al., 2017). The methodology in this study included a collection interval of 2 m both horizontally and vertically across the study plot, for a total of 60 rainfall collectors; this density accounted for the great spatial variability of *Tf* underneath forest canopies (Sadeghi et al., 2015). The cumulative observed Tf over the two seasons was 420.4 mm (*Tf*/*P* = 56.4% of the total rainfall) for this study area; this value was lower than that found at 2700 m elevation (approximately *Tf*/*P* = 64.7%) by He et al. (2014), and in other studies in tropical and temperate forest regions (Carlyle-Moses et al., 2010; Fathizadeh et al., 2017), but higher than that of Sadeghi et al. (2015) (average value of 43.9% for *Pinus eldarica* in Northern Iran with an average annual rainfall of 272 mm). According to Horton (1919) and Sadeghi et al. (2015), the size of *P* was a primary control factor of the differences in *Tf*/*P* across studies. This was also observed in this study (Table 1), with largest *I*/*P* for smallest rainfall events; also, a

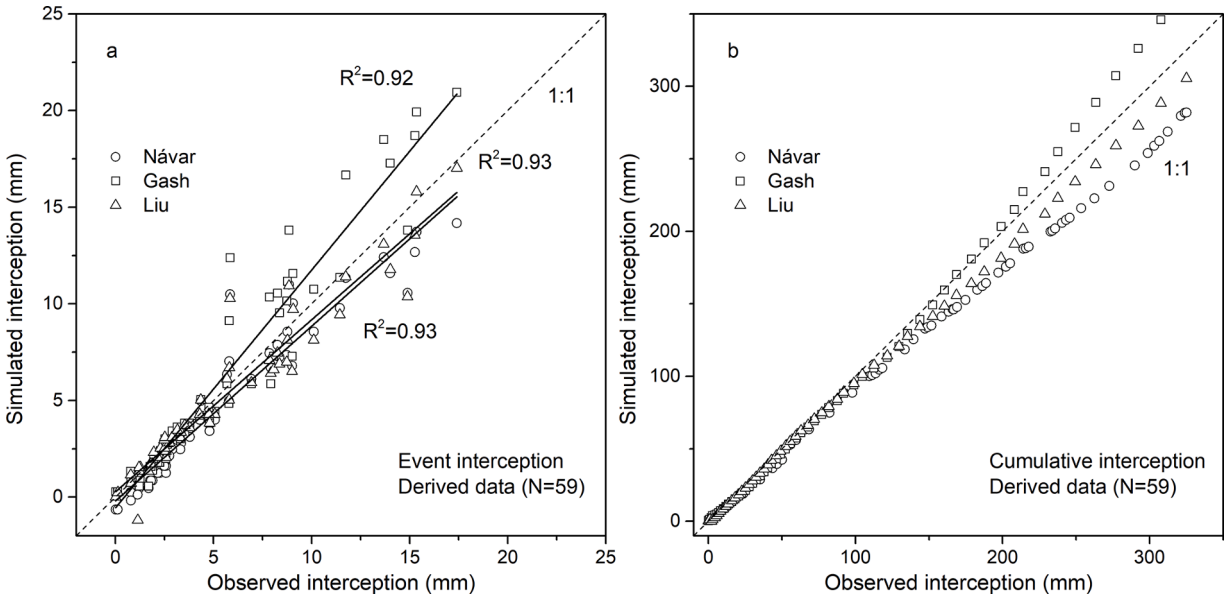


**Fig. 6.** The relationships between the observed and simulated interception for event (a) and cumulative rainfall (b) for the entire period using three models (N means the number of rainfall events used for statistics).

**Table 5**
The average bias of the event-based interception analysis with the three models.

| Model | Interception bias event-based (mm) | Percentage bias event-based (%) |
|---|---|---|
| Power Návar model | −0.73 | −13.3% |
| Reformulated Gash model | 0.71 | 12.9% |
| Reformulated Liu model | −0.27 | −4.9% |

higher frequency of very small and small rainfall (with a total of 57.5% based-event) reduced the *Tf/P* ratio.

*Sf* quantities are highly variable between and within different vegetation types (Levia and Frost, 2003). Stemflow accounted for 8.4% of *P* in this study, 11.2% in a *Pinus radiata* plantation in Upper Yass Representative Basin in Australia with a mean annual rainfall of 679 mm (Crockford and Richardson (1990), and 6.2% in young *P. altissima* trees (Prasad Ghimire et al., 2017). Most species with a rough bark exhibited low *Sf* (Licata et al., 2011; Navar, 1993; Sadeghi et al., 2020; Valente et al., 1997; Xiangyang et al., 2013), while trees with a smooth bark and DBHs from 10 to 20 cm (17.3 ± 6.4 cm in this study) contributed high *Sf* in the Cerrado savanna of Brazil, (Tonello et al. (2021). Jeong et al. (2020) observed that, generally, the greater the rainfall, the higher the *Sf/P*; the amount of C6 varying from 14.5 to > 36.5% in this study. The maximum rainfall observed was 40.8 to 51.3 mm in growing season one and two, respectively, suggesting that the increase in extreme rainfall events may be the reason for the high *Sf*. Meanwhile, the probability of *Sf* was only 0.3 for a 42 mm rainfall (Figs. 2 and 3), illustrating that occurrence of *Sf* in a *P. crassifolia* forest is not a common event, even with extreme weather.

*I* accounted for 35.2% of *P* and that was consistent with observations of He et al. (2014) in the same area at 2700 m, and in Sitka spruce in Sweden (Alavi et al., 2001). The similarities were likely related to canopy characteristics (eg. LAI, crown openness, and crown length). LAI was 2.72 and 2.49 and canopy cover was 0.85 and 0.83 at 3000 and 2700 m, respectively. The higher frequency of C1 and C2 events from 37.3 to 57.6% (Table 1) may be more convincing of the variousness in *I* (Prasad Ghimire et al., 2017). The *S* value at 3000 m was higher (2.0) than at 2700 m (1.61) (He et al., 2014), and similar to *S* from other needle-leaved species (Llorens and Gallart, 2000; Motahari et al., 2013). The dissimilarity in *S* can be clarified by the higher LAI (2.72) and higher canopy cover 0.85 in the present study (Sadeghi et al., 2015). *p* in this study was calculated as 0.15, which was very close to the 0.1 in *P. eldarica* stands (Motahari et al., 2013). Overall, a higher *S* as well as lower *p* values in *P. crassifolia* resulted in high interception in this semi-arid region and a reduced runoff from the local forest area.

*Model performance and evaluation.* A linear or a power regression equation have commonly described the *I* vs. *P* relationship depending on forest types, climate, and rainfall conditions (Návar, 2019; Návar and Bryan, 1990). The NSEs for linear and power Návar models in this study were −4.04 and 0.90, respectively, indicating a better fit of the power than of the linear model (Table 3 and Fig. 6), further, $E_p$ (a function of *P* linear and Power regression equations) decayed rapidly over *P*, that is, there was an abatement of local and advected sensible heat over *P* or time (Návar, 2020). Parameters in the Návar model were initialized with a reference value for arid and semi-arid regions Návar (2020), and $R^2$, MRAE, and NSE were 0.89, 0.32 and 0.86, respectively, indicating a reasonable, but not sufficiently good fit. To optimize the evaluation, we derived the most appropriate parameters and finally obtained a 'very good' modeling result compared with the other two physical models (Tables 3 and 4). The $R^2$ between the observed and modeled values was the same among the three models at 0.93, with differing absolute mean errors, and a smaller deviation in the Návar model; this was consistent with reported statistics for most forests around the world (Muzylo et al., 2009). The Liu model yielded a larger MRAE of 0.59. The Gash model had a larger deviation during large and very large storms, but *I* prediction was consistent with the observed values (NSE=0.92). That is, the Liu and Návar models appear to be well suited for *I* simulation in spruce stands in semi-arid climate. The performance of NSE was better than that obtained by Návar (2019) and Návar (2020) for a semi-arid region. The cumulative interception loss at the scale of a case study resulted in an excellent fit for the three models used, and with an ideal evaluation index value (Table 4).

Compared to previous studies (Motahari et al., 2013; Muzylo et al., 2009; Prasad Ghimire et al., 2017), the error for *I* estimation can be up to 20%. The Návar model with NSE of 0.93 was slightly inferior to the other two models (NSE of 0.98 and 0.99, respectively). The Návar model focuses on event-based interception, while the Gash and Liu model uses cumulative rain volumes; this indicates that the Návar model is more appropriate for event-based interception modeling, while the Liu model would be a better selection for total interception modeling.

**Table 6**
Summary statistics for the performance of three models in modeling measured interception (*I*) against on event-based rainfall analysis.

| Classification of rainfall | Power Návar model | | | Reformulated Gash model | | | Reformulated Liu model | | | |
|---|---|---|---|---|---|---|---|---|---|---|
| | $R^2$ | MRAE | NSE | $R^2$ | MRAE | NSE | $R^2$ | MRAE | NSE | Number |
| C1 | 0.91 | 0.09 | 0.29 | 0.79 | 0.26 | 0.74 | 0.69 | 0.71 | 0.53 | 22 |
| C2 | 0.84 | 0.04 | −0.31 | 0.78 | 0.06 | 0.72 | 0.83 | 0.04 | 0.70 | 12 |
| C3 | 0.34 | 0.05 | −1.78 | 0.34 | 0.06 | 0.24 | 0.36 | 0.05 | 0.33 | 4 |
| C4 | 0.02 | 0.03 | −0.50 | 0.00 | 0.18 | −4.09 | 0.01 | 0.04 | −1.72 | 8 |
| C5 | 0.04 | 0.07 | −0.15 | 0.21 | 0.07 | −0.23 | 0.02 | 0.09 | −0.07 | 6 |
| C6 | 0.78 | 0.03 | 0.58 | 0.94 | 0.03 | −1.76 | 0.74 | 0.07 | 0.72 | 7 |

To better understand how the three models perform, we quantitatively evaluated model accuracy for different rainfall events (Table 6). We found similarities among the three models, and they performed consistently well for class C1, C2, and C6, which accounted for 70% of total rainfall events; the models did not perform as well for class C3, C4, and C5 ($R^2$<0.5). Most of NSEs were negative for the three classes, which indicated that the observed mean was a better predictor than the model, and the model did not predict *I* well, as previously described by other scientists (Crockford and Richardson, 2000; Nazari et al., 2020; Panahandeh et al., 2022; Sadeghi et al., 2015). This demonstrated that the model can be further improved by simulating large rain storms (i.e., post-saturation point), in which *I* is not simply dependent on *P, S* and the canopy cover fraction (*c*), but also on the mean of the ratio of evaporation to the mean of rainfall intensity (Panahandeh et al., 2022). On the other hand, the lack of large rain storm records lead to insufficient *I* data, which created highly uncertain data of the interception event, and led to insignificant statistical results or even a negative value. The performance for the classified rainfall was slightly different than for event-based interception (Fig. 6a). Two reasons may account for this. First, large rainfall events do not necessarily result in large interception, and, second, density of the rainfall events was different. We conclude that the understanding of potential influences of the interception process and classified rainfall events would require more data of higher resolution. Overall, our results showed that the performance of interception modeling of classified rainfall events varies among the three models.

## 5. Conclusions

Field observation and prediction models are both important in a multidisciplinary effort to quantify and balance ecosystem and human water utilization in an uncertain climate forecast in arid and semi-arid regions. Based on the parameterization of interception components and canopy structural traits, we recommend the Návar and the reformulated Liu model for estimating event-based and total *I* in the semi-arid coniferous *P. crassifolia* forest. Direct measures of canopy structural parameters and trial-and-error can greatly improve the simulation effect of the physical model. This is a study of rainfall interception modeling at an individual elevation (plot scale) in a mountain forest. Future research may explore differences in parametric schemes and simulations of canopy interception at different elevations, improving simulations at watershed and regional scales. The effect of *I* at the 3000 m elevation indicated that less rainfall was available for infiltration and recharge at the high-altitude forest area due to high rates of evaporation. Based on the parameters and models recommended in this study, local forest management departments can better predict hydrological processes, such as forest land runoff and flow confluence processes under extreme rainfall events.

## Declaration of Competing Interest

The authors declare that they have no known competing financial interests or personal relationships that could have appeared to influence the work reported in this paper.

## Data Availability

Data will be made available on request.

## Acknowledgment

This work was supported by the National Science Foundation: 41901050 and 41901044 Strategic Priority Program of the Chinese Academy of Sciences, Grant or Award Number: XDA23060301. We also appreciate the reviewers' constructive and valuable suggestions for model calibration.

## References

Alavi, G., Jansson, P.-.E., Hällgren, J.-.E., Bergholm, J., 2001. Interception of a dense spruce forest, performance of a simplified canopy water balance model. Hydrol. Res. 32 (4–5), 265–284. https://doi.org/10.2166/nh.2001.0016.

Calder, I.R., 1976. The measurement of water losses from a forested area using a "natural" lysimeter. J. Hydrol. 30 (4), 311–325. https://doi.org/10.1016/0022-1694(76)90115-3.

Carlyle-Moses, D.E., Park, A.D., Cameron, J.L., 2010. Modelling rainfall interception loss in forest restoration trials in Panama. Ecohydrology 3 (3), 272–283. https://doi.org/10.1002/eco.105.

Carlyle-Moses, D.E., Price, A.G., 2007. Modelling canopy interception loss from a Madrean pine-oak stand, northeastern Mexico. Hydrol. Process. 21 (19), 2572–2580. https://doi.org/10.1002/hyp.6790.

Chang, X.X., et al., 2014. Qinghai spruce (Picea crassifolia) forest transpiration and canopy conductance in the upper Heihe River Basin of arid northwestern China. Agric. For. Meteorol. 198, 209–220. https://doi.org/10.1016/j.agrformet.2014.08.015.

Crockford, R.H., Richardson, D.P., 1990. Partitioning of rainfall in a eucalypt forest and pine plantation in southeastern australia: I throughfall measurement in a eucalypt forest: effect of method and species composition. Hydrol. Process. 4 (2), 131–144. https://doi.org/10.1002/hyp.3360040204.

Crockford, R.H., Richardson, D.P., 2000. Partitioning of rainfall into throughfall, stemflow and interception: effect of forest type, ground cover and climate. Hydrol. Process. 14 (16–17), 2903–2920. https://doi.org/10.1002/1099-1085(200011/12)14, 16/17<2903::AID-HYP126>3.0.CO;2-6.

Cuartas, L.A., et al., 2007. Interception water-partitioning dynamics for a pristine rainforest in Central Amazonia: marked differences between normal and dry years. Agric. For. Meteorol. 145 (1–2), 69–83. https://doi.org/10.1016/j.agrformet.2007.04.008.

Deguchi, A., Hattori, S., Park, H.T., 2006. The influence of seasonal changes in canopy structure on interception loss: application of the revised Gash model. J. Hydrol. 318 (1–4), 80–102. https://doi.org/10.1016/j.jhydrol.2005.06.005.

Eliades, M., et al., 2022. Testing three rainfall interception models and different parameterization methods with data from an open Mediterranean pine forest. Agric. For. Meteorol. 313, 108755 https://doi.org/10.1016/j.agrformet.2021.108755.

Fan, J.L., Oestergaard, K.T., Guyot, A., Lockington, D.A., 2014. Measuring and modeling rainfall interception losses by a native Banksia woodland and an exotic pine plantation in subtropical coastal Australia. J. Hydrol. 515, 156–165. https://doi.org/10.1016/j.jhydrol.2014.04.066.

Fathizadeh, O., Hosseini, S.M., Zimmermann, A., Keim, R.F., Darvishi Boloorani, A., 2017. Estimating linkages between forest structural variables and rainfall interception parameters in semi-arid deciduous oak forest stands. Sci. Total Environ. 601-602, 1824–1837. https://doi.org/10.1016/j.scitotenv.2017.05.233.

Gash, J.H.C., 1979. An analytical model of rainfall interception in forests. Q. J. Roy. Meteor. Soc. 105, 43–55. https://doi.org/10.1002/qj.49710544304.

Gash, J.H.C., Lloyd, C.R., Lachaud, G., 1995. Estimating sparse forest rainfall interception with an analytical model. J. Hydrol. 170 (1–4), 79–86. https://doi.org/10.1016/0022-1694(95)02697-N.

Gill, M.K., Kaheil, Y.H., Khalil, A., McKee, M., Bastidas, L., 2006. Multiobjective particle swarm optimization for parameter estimation in hydrology. Water Resour. Res. 42 (7) https://doi.org/10.1029/2005WR004528.

Grunicke, S., Queck, R., Bernhofer, C., 2020. Long-term investigation of forest canopy rainfall interception for a spruce stand. Agric. For. Meteorol. 292-293, 108125 https://doi.org/10.1016/j.agrformet.2020.108125.

He, Z.B., et al., 2014. Spatial variability of canopy interception in a spruce forest of the semiarid mountain regions of China. Agric. For. Meteorol. 188, 58–63. https://doi.org/10.1016/j.agrformet.2013.12.008.

Horton, R.E., 1919. Rainfall interception. Mon. Weather Rev. 47, 603–623 dx.doi.org/10.

Jeong, S., Otsuki, K., Shinohara, Y., Inoue, A., Ichihashi, R., 2020. Stemflow estimation models for Japanese cedar and cypress plantations using common forest inventory data. Agric. For. Meteorol. 290, 107997 https://doi.org/10.1016/j.agrformet.2020.107997.

Jian, S., Hu, C., Zhang, G., Zhang, J., 2019. Study on the throughfall, stemflow, and interception of two shrubs in the semiarid Loess region of China. Agric. For. Meteorol. 279, 107713 https://doi.org/10.1016/j.agrformet.2019.107713.

Junqueira Junior, J.A., et al., 2019. Rainfall partitioning measurement and rainfall interception modelling in a tropical semi-deciduous Atlantic forest remnant. Agric. For. Meteorol. 275, 170–183. https://doi.org/10.1016/j.agrformet.2019.05.016.

Klaassen, W., Bosveld, F., de Water, E., 1998. Water storage and evaporation as constituents of rainfall interception. J. Hydrol. 212-213, 36–50. https://doi.org/10.1016/S0022-1694(98)00200-5.

Levia, D.F., Frost, E.E., 2003. A review and evaluation of stemflow literature in the hydrologic and biogeochemical cycles of forested and agricultural ecosystems. J. Hydrol. 274 (1–4), 1–29. https://doi.org/10.1016/S0022-1694(02)00399-2.

Licata, J.A., et al., 2011. Decreased rainfall interception balances increased transpiration in exotic ponderosa pine plantations compared with native cypress stands in Patagonia, Argentina. Ecohydrology 4 (1), 83–93. https://doi.org/10.1002/eco.125.

Linhoss, A.C., Siegert, C.M., 2016. A comparison of five forest interception models using global sensitivity and uncertainty analysis. J. Hydrol. 538, 109–116. https://doi.org/10.1016/j.jhydrol.2016.04.011.

Liu, S., 1997. A new model for the prediction of rainfall interception in forest canopies. Ecol. Model. 99 (2), 151–159. https://doi.org/10.1016/S0304-3800(97)01948-0.

Llorens, P., Gallart, F., 2000. A simplified method for forest water storage capacity measurement. J. Hydrol. 240 (1), 131–144. https://doi.org/10.1016/S0022-1694(00)00339-5.

Ma, C., Luo, Y., Shao, M., 2020. Comparative modeling of the effect of thinning on canopy interception loss in a semiarid black locust (Robinia pseudoacacia) plantation in Northwest China. J. Hydrol. 590, 125234 https://doi.org/10.1016/j.jhydrol.2020.125234.

Motahari, M., Attarod, P., Pypker, T.G., Etemad, V., Shirvany, A., 2013. Rainfall Interception in a Pinus eldarica Plantation in a Semi-arid Climate Zone: an Application of the Gash Model. J. Agr. Sci. Tech-Iran 15 (5), 981–994.

Muzylo, A., et al., 2009. A review of rainfall interception modelling. J. Hydrol. 370 (1), 191–206. https://doi.org/10.1016/j.jhydrol.2009.02.058.

W. N. Moriasi, D., Gitau, M., Pai, N., Daggupati, P., 2015. Hydrologic and water quality models: performance measures and evaluation criteria T ASABE 58 (6), 1763–1785. https://doi.org/10.13031/trans.58.10715.

Nash, J.E., Sutcliffe, J.V., 1970. River flow forecasting through conceptual models part I A discussion of principles. J. Hydrol. (Amst.) 10, 282–290.

Navar, J., 1993. The causes of stemflow variation in 3 semiarid growing species of northeastern mexico. J. Hydrol. 145 (1–2), 175–190. https://doi.org/10.1016/0022-1694(93)90226-Y.

Návar, J., 2019. Modeling rainfall interception components of forests: extending drip equations. Agric. For. Meteorol. 279, 107704 https://doi.org/10.1016/j.agrformet.2019.107704.

Návar, J., 2020. Modeling rainfall interception loss components of forests. J. Hydrol. 584, 124449 https://doi.org/10.1016/j.jhydrol.2019.124449.

Návar, J., Bryan, R., 1990. Interception loss and rainfall redistribution by three semi-arid growing shrubs in northeastern Mexico. J. Hydrol. 115 (1), 51–63. https://doi.org/10.1016/0022-1694(90)90197-6.

Nazari, M., Sadeghi, S.M.M., Van Stan, J.T., Chaichi, M.R., 2020. Rainfall interception and redistribution by maize farmland in central Iran. J. Hydrol.: Regional Studies 27, 100656. https://doi.org/10.1016/j.ejrh.2019.100656.

Nourani, V., Baghanam, A.H., Adamowski, J., Kisi, O., 2014. Applications of hybrid wavelet-Artificial Intelligence models in hydrology: a review. J. Hydrol. 514, 358–377. https://doi.org/10.1016/j.jhydrol.2014.03.057.

Panahandeh, T., et al., 2022. The performance of the reformulated Gash rainfall interception model in the Hyrcanian temperate forests of northern Iran. J. Hydrol. (Amst.) 612, 128092. https://doi.org/10.1016/j.jhydrol.2022.128092.

Prasad Ghimire, C., et al., 2017. Measurement and modeling of rainfall interception by two differently aged secondary forests in upland eastern Madagascar. J. Hydrol. 545, 212–225. https://doi.org/10.1016/j.jhydrol.2016.10.032.

Pypker, T.G., Tarasoff, C.S., Koh, H.-.S., 2012. Assessing the efficacy of two indirect methods for quantifying canopy variables associated with the interception loss of rainfall in temperate hardwood forests. OJMH 2 (2), 12. https://doi.org/10.4236/ojmh.2012.22005.

Qubaja, R., et al., 2020. Partitioning evapotranspiration and its long-term evolution in a dry pine forest using measurement-based estimates of soil evaporation. Agric. For. Meteorol. 281, 107831 https://doi.org/10.1016/j.agrformet.2019.107831.

Raz-Yaseef, N., Rotenberg, E., Yakir, D., 2010. Effects of spatial variations in soil evaporation caused by tree shading on water flux partitioning in a semi-arid pine forest. Agric. For. Meteorol. 150 (3), 454–462. https://doi.org/10.1016/j.agrformet.2010.01.010.

Rotenberg, E., Yakir, D., 2010. Contribution of semi-arid forests to the climate system. Science 327 (5964), 451–454. https://doi.org/10.1126/science.1179998.

Rutter, A.J., Robins, P.C., Morton, A.J., Kershaw, K.A., 1972. A predictive model of rainfall interception in forests, 1. Derivation of the model from observations in a plantation of Corsican pine. Agric. Meteorol. 9 (5–6) https://doi.org/10.1016/0002-1571(71)90034-3, 367-&.

Sadeghi, S.M.M., Attarod, P., Van Stan II, J.T., Pypker, T.G., Dunkerley, D., 2015. Efficiency of the reformulated Gash's interception model in semiarid afforestations. Agric. For. Meteorol. 201, 76–85. https://doi.org/10.1016/j.agrformet.2014.10.006.

Sadeghi, S.M.M., Gordon, D. and Van Stan, J., 2020. A Global Synthesis of Throughfall and Stemflow Hydrometeorology, 49–70 pp. 10.1007/978-3-030-29702-2_4.

Tonello, K.C., et al., 2021. Stemflow variability across tree stem and canopy traits in the Brazilian Cerrado. Agric. For. Meteorol. 308-309, 108551 https://doi.org/10.1016/j.agrformet.2021.108551.

Valente, F., David, J.S., Gash, J.H.C., 1997. Modelling interception loss for two sparse eucalypt and pine forests in central Portugal using reformulated Rutter and Gash analytical models. J. Hydrol. 190 (1), 141–162. https://doi.org/10.1016/S0022-1694(96)03066-1.

Xiangyang, S., Wang, G., Lin, Y., Liu, L., Gao, Y., 2013. Intercepted rainfall in Abies fabri forest with different-aged stands in Southwest China. Turk. J. Agric. For. 37, 495–504. https://doi.org/10.3906/tar-1207-36.

Yang, J.J., et al., 2016. Assessing artificial neural networks coupled with wavelet analysis for multi-layer soil moisture dynamics prediction. Sci. Cold Arid Reg. 8 (2), 116–124. http://www.scar.ac.cn/EN/10.3724/SP.J.1226.2016.00116.